

# Extra DoF of Near-Field Holographic MIMO Communications Leveraging Evanescent Waves

Ran Ji, Shuo Chen, Chongwen Huang<sup>1</sup>, *Member, IEEE*, Jun Yang<sup>2</sup>, Wei E. I. Sha<sup>3</sup>, *Senior Member, IEEE*, Zhaoyang Zhang<sup>4</sup>, *Senior Member, IEEE*, Chau Yuen<sup>5</sup>, *Fellow, IEEE*, and Mérouane Debbah, *Fellow, IEEE*

**Abstract**—In this letter, we consider transceivers with spatially-constrained antenna apertures of rectangular symmetry, and aim to improve of spatial degrees of freedom (DoF) and channel capacity leveraging evanescent waves for information transmission in near-field scenarios based on the Fourier plane-wave series expansion. The treatment is limited to an isotropic scattering environment but can be extended to the non-isotropic case through the linear-system theoretic interpretation of plane-wave propagation. Numerical results show that evanescent waves have the significant potential to provide additional DoF and capacity in the reactive near-field region.

**Index Terms**—Spatial degrees of freedom, channel capacity, evanescent wave, physics-based channel modeling.

## I. INTRODUCTION

IN MIMO (multiple-input multiple-output) systems, channel capacity grows linearly with the number of spatial degrees of freedom (DoF), which is relative to both the scattering environment and antenna array geometries. Recently, the concept of *holographic MIMO (HMIMO)* has drawn increasing attention and is regarded as one of the possible technologies used in 6G communications [1]. A HMIMO array consists of a massive (possible infinite) number of antennas integrating into a compact space, which can be seen as an ultimate form of spatially-constrained MIMO system and be modeled as spatially-continuous electromagnetic (EM) apertures with asymptotically infinite antennas. Thus, a fundamental question of holographic communications is to obtain the

number of spatial DoF and capacity of a HMIMO system. To answer this question, many previous works have investigated the continuous-space channel modeling under different propagation conditions and array geometries, e.g., [2], [3], [4]. However, these models are all based on the far-field communication assumption, which might be not applicable with dramatic increase of antenna aperture and higher operation frequencies that make near-field communications be the practical scenario. Thus, near-field modeling, the spatial DoF and its capacity boundary are needed. There have been some works trying to fill the gap from the Green's function and electromagnetic theory, such as [5], [6] and [7]. In these works, the authors derive channel models and estimate near-field communication performances from Green's function, corresponding to a relatively simple communication scenario. However, to the best of the authors' knowledge, near-field analysis based on channel model corresponding to complex scattering environment have not been investigated.

In this letter, we consider transceivers with spatially-constrained antenna apertures of rectangular symmetry in spatially-stationary monochromatic scattering propagation environment. Unlike work [8] that a Fourier orthonormal expansion was derived to compute the DoF limit in the far-field region, we focus on the reactive near-field communication scenario and compute the DoF and capacity gain by considering evanescent waves. To the best of our knowledge, this is the initial work to analyze the DoF and capacity limit of the near-field communications under a generalized stochastic spatially-stationary monochromatic channel. Moreover, we also demonstrate our proposition through numerical simulations and verify its coherence with traditional results, i.e., the maximum DoF and capacity of the far-field communication that are provided in [8] and [9]. Specifically, we take full potential of evanescent waves in reactive near-field holographic communications, and drive its extra DoF and capacity based on Fourier plane-wave series expansion. Numerical results show that the DoF and capacity of reactive near-field communications can be improved by 30% respectively comparing with the traditional far-field scenario.

## II. SYSTEM MODEL

We study a holographic communication system where the transmitter and the receiver are equipped with planar HMIMO surface. Considering the electromagnetic wave propagation in every direction (i.e., isotropic propagation) through a homogeneous, isotropic, and infinite random scattered medium, the 3D small-scale fading channel can be modeled as a

Manuscript received 27 November 2022; accepted 29 December 2022. Date of publication 3 January 2023; date of current version 11 April 2023. This work was supported in part by the China National Key Research and Development Program under Grant 2021YFA1000500; in part by the National Natural Science Foundation of China under Grant 62101492; in part by the Zhejiang Provincial Natural Science Foundation of China under Grant LR22F010002; in part by the National Natural Science Fund for Excellent Young Scientists Fund Program (Overseas); in part by the Zhejiang University Education Foundation Qizhen Scholar Foundation; in part by the Fundamental Research Funds for the Central Universities under Grant 2021FZZX001-21; and in part by the Ministry of Education, Singapore, under its MOE Tier 2 under Award MOE-T2EP50220-0019. The associate editor coordinating the review of this article and approving it for publication was C. Psomas. (*Corresponding author: Chongwen Huang.*)

Ran Ji, Shuo Chen, Chongwen Huang, Wei E. I. Sha, and Zhaoyang Zhang are with the College of Information Science and Electronic Engineering, Zhejiang University, Hangzhou 310000, China (e-mail: chongwenhuang@zju.edu.cn).

Jun Yang is with the Wireless Product Research and Development Institute, ZTE Corporation, Shenzhen 518057, China.

Chau Yuen is with the Engineering Product Development, Singapore University of Technology and Design, Singapore 119613.

Mérouane Debbah is with the AI and Digital Science Research Center, Technology Innovation Institute, Abu Dhabi, UAE.

Digital Object Identifier 10.1109/LWC.2023.3234003

zero-mean, spatially-stationary and Gaussian random field  $h_{\omega}(x, y, z) : (x, y, z) \in \mathbb{R}^3$  [9], [10]: It is a function of frequency and spatial position  $(x, y, z)$ . Since we only consider monochromatic waves in this letter, the variant  $\omega$  can thus be omitted. This channel can be completely described according to [10]:

$$c_h(x, y, z) = \mathbb{E}\{h^*(x', y', z')h(x + x', y + y', z + z')\} \quad (1)$$

$$S_h(k_x, k_y, k_z) = \iiint c_h(x, y, z)e^{-j(k_x x + k_y y + k_z z)} dx dy dz \quad (2)$$

where  $c_h(x, y, z)$  is the spatial auto-correlation function in spatial domain and  $S_h(k_x, k_y, k_z)$  is the power spectral density in wave-number domain.

#### A. Fourier Plane-Wave Spectral Representation

In a source-free environment, the EM nature of small-scale fading requires realizations of  $h(x, y, z)$  to satisfy scalar Helmholtz equation in frequency domain, which can be seen as a constraint of  $h(x, y, z) : (\nabla^2 + \kappa^2)h(x, y, z) = 0$  where  $\kappa = \frac{2\pi}{\lambda}$  is the module of the vector wave-number and  $\lambda$  is the wavelength. Following the derivation in [10], [11],  $h(x, y, z)$  is decomposed into the sum of two random fields:

$$h(x, y, z) = h_+(x, y, z) + h_-(x, y, z) \quad (3)$$

which is further defined as the *Fourier plane-wave spectral representation*:

$$h_{\pm}(x, y, z) = \frac{1}{4\pi\sqrt{\pi}} \iint \sqrt{S_h(k_x, k_y)} W^{\pm}(k_x, k_y) \times e^{j(k_x x + k_y y \pm \gamma(\kappa_x, \kappa_y)z)} \quad (4)$$

with

$$\gamma(k_x, k_y) = \sqrt{\kappa^2 - k_x^2 - k_y^2} \quad (5)$$

where  $W^+(k_x, k_y)$  and  $W^-(k_x, k_y)$  are two 2D independent, zero-mean, complex-valued, white-noise Gaussian random fields,  $S_h(k_x, k_y)$  is the 2D power spectral density of  $h_{\pm}(x, y, z = 0)$ . Conventionally,  $S_h(k_x, k_y)$  is defined over a compact support  $k_x^2 + k_y^2 \leq \kappa^2$  given by a disk of radius  $\kappa$  centered on the origin (excluding a purely imaginary  $\gamma(k_x, k_y)$  that is called evanescent wave because it does not contribute to far-field propagation). This limits the bandwidth of conventional  $h(x, y, z)$  (in wavenumber domain) to  $\pi\kappa^2$ . However, as we will demonstrate in Section IV, the far-field communication assumption might be not applicable in some short range communication scenarios because of the increase of antenna aperture and operating frequencies in next generation communication. As a consequence, it is possible to leverage evanescent EM waves to transmit information in near-field communications.

#### B. 4D Fourier Plane-Wave Series Expansion

Different from describing spatial fading characteristics at different points as above, in [9], authors proposed 4D Fourier plane-wave representation and 4D Fourier plane-wave series expansion of EM channels relative to two spatial points.

Specifically, 4D Fourier plane-wave representation can be written as

$$h(\mathbf{r}, \mathbf{s}) = \frac{1}{(2\pi)^2} \iiint \iiint a_r(\mathbf{k}, \mathbf{r}) H_a(k_x, k_y, \kappa_x, \kappa_y) a_s(\boldsymbol{\kappa}, \mathbf{s}) \times dk_x dk_y d\kappa_x d\kappa_y \quad (6)$$

where the spatial channel is decomposed into three terms. The first and third terms are receive response and source response, respectively. The source response maps the excitation currents in the transmitting volume into the transmitted field with propagation direction  $\hat{\boldsymbol{\kappa}} = \boldsymbol{\kappa}/\|\boldsymbol{\kappa}\|$ . Similarly, the receive response's role is analogous to the source response, except that it maps the receive field to the induced current in the receiving volume. These two functions are defined as follow:  $a_r(\mathbf{k}, \mathbf{r}) = e^{j\mathbf{k}^T \mathbf{r}} = e^{j(k_x r_x + k_y r_y + \gamma(k_x, k_y)r_z)}$ ;  $a_s(\boldsymbol{\kappa}, \mathbf{s}) = e^{-j\boldsymbol{\kappa}^T \mathbf{s}} = e^{-j(\kappa_x r_x + \kappa_y r_y + \gamma(\kappa_x, \kappa_y)r_z)}$ . The second term  $H_a(k_x, k_y, \kappa_x, \kappa_y)$  is defined as angular response, describing the channel coupling between different pairs of transmitting direction  $\boldsymbol{\kappa}$  and receiving direction  $\mathbf{k}$ .

Furthermore, to facilitate calculation and simulation, 4D Fourier plane-wave series expansion is proposed to approximate (6):

$$h(\mathbf{r}, \mathbf{s}) \approx \sum_{(l_x, l_y) \in \mathcal{E}_R} \sum_{(m_x, m_y) \in \mathcal{E}_S} a_r(l_x, l_y, \mathbf{r}) H_a(l_x, l_y, m_x, m_y) a_s(l_x, l_y, \mathbf{s}) \quad (7)$$

where  $a_r(l_x, l_y, \mathbf{r}) = e^{j(\frac{2\pi}{L_{R,x}} l_x r_x + \frac{2\pi}{L_{R,y}} l_y r_y + \gamma_r(l_x, l_y)r_z)}$  and  $a_s(m_x, m_y, \mathbf{s}) = e^{-j(\frac{2\pi}{L_{S,x}} m_x s_x + \frac{2\pi}{L_{S,y}} m_y s_y + \gamma_r(m_x, m_y)s_z)}$  are discretized receive and source response obtained by evaluating  $(k_x, k_y)$  at  $(\frac{2\pi l_x}{L_{R,x}}, \frac{2\pi l_y}{L_{R,y}})$  and  $(\kappa_x, \kappa_y)$  at  $(\frac{2\pi m_x}{L_{S,x}}, \frac{2\pi m_y}{L_{S,y}})$ . Angular response  $H_a(l_x, l_y, m_x, m_y)$  can be modeled as statistically independent, circularly-symmetric, complex-Gaussian random variables with different variances depending on power spectral density.  $\mathcal{E}_R$  is the support of  $H_a(l_x, l_y, m_x, m_y)$  excluding evanescent waves, resulting in the following constraint:  $\mathcal{E}_R = [(l_x, l_y \in \mathbb{Z}^2) : (\frac{l_x \lambda}{L_{R,x}}) + (\frac{l_y \lambda}{L_{R,y}}) \leq 1]$ . And it is the same for  $\mathcal{E}_S$ .

The channel matrix of HMIMO communications can be written as

$$\mathbf{H} = \boldsymbol{\Phi}_R \tilde{\mathbf{H}} \boldsymbol{\Phi}_S^H = \boldsymbol{\Phi}_R e^{j\boldsymbol{\Gamma}_R} \mathbf{H}_a e^{-j\boldsymbol{\Gamma}_S} \boldsymbol{\Phi}_S^H \quad (8)$$

where  $\boldsymbol{\Gamma}_R = \text{diag}(\boldsymbol{\gamma}_R) r_z$  and  $\boldsymbol{\Gamma}_S = \text{diag}(\boldsymbol{\gamma}_S) s_z$ .  $\boldsymbol{\Phi}_R$  and  $\boldsymbol{\Phi}_S$  are 2D spatial-frequency Fourier harmonics matrix of dimension  $N_R \times n_R$  and  $N_S \times n_S$ , respectively.  $N_R$  and  $N_S$  are antenna elements on HMIMO surfaces and  $n_R$  and  $n_S$  represent numbers of wavenumber domain sampling points in  $\mathcal{E}_R$  and  $\mathcal{E}_S$ , respectively.  $\boldsymbol{\Phi}_R$  is composed of vectors  $\boldsymbol{\phi}_R(l_x, l_y) \in \mathbb{C}^{N_R}$  with entries  $[\boldsymbol{\phi}_R(l_x, l_y)]_j = e^{-j(\frac{2\pi}{L_{R,x}} l_x r_{xj} + \frac{2\pi}{L_{R,y}} l_y r_{yj})}$ . And it is the same for the transmitter.

### III. DOF AND CAPACITY OF NEAR-FIELD HOLOGRAPHIC MIMO COMMUNICATIONS

In electromagnetics, an evanescent field, or evanescent wave, is an oscillating electric and/or magnetic field that does not propagate as an EM wave but whose energy is spatially concentrated in the vicinity of the source. As we can see that

the DoF of HMIMO channels in far-field communication scenarios has been computed in [8], but evanescent waves are not considered since they attenuate exponentially with the distance. When we go to beyond 5G or 6G communications with HMIMO surfaces under higher operating frequencies, i.e., millimeter wave or terahertz, the original far-field communication scenario will become a near-field one according to the Raleigh distance  $\frac{2D^2}{\lambda}$ , where  $D$  is the maximum linear dimension of the antenna, and  $\lambda$  is the wavelength of the EM waves. One typical scenario is that the whole wall of an indoor room is equipped with HMIMO surfaces as the transmitter using sufficiently high carrier frequencies for communications, which might make the whole indoor environment fall in transmitter's near-field region. For example, using a carrier frequency  $f = 5$  GHz (i.e.,  $\lambda = 6$  cm) and HMIMO surface aperture length  $L_x = L_y = 1$  m, this roughly provide a near-field range of  $2D^2/\lambda \approx 33.3$  m. Specifically, electromagnetic near-field can be further divided into reactive near-field and radiative near-field. Even we only considers the reactive near-field, where evanescent waves are the strongest, its range is up to  $0.62\sqrt{\frac{D^3}{\lambda}} = 2.53$  m.

When using HMIMO surfaces to control the EM wave, the reflected wave are usually off the surface at an angle greater than the critical angle where evanescent waves are formed. This only happens in the near field since the intensity of evanescent waves decays exponentially with the distance from the interface at which they are formed. Therefore, it is natural to consider of using evanescent wave to carry information besides the normal plane waves that can be applied for information transmission in the original far-field range. In this letter, we compute the limit of the average number of spatial DoF and capacity with evanescent waves. Furthermore, we will show that evanescent waves can bring the considerable DoF and capacity gain in reactive near field region from both theoretical and numerical perspectives.

### A. Degrees of Freedom

1) *Far-Field Communications*: It is well known that a band limited orthonormal series expansion has a countably-finite number of coefficients, whose cardinality determines the space dimension [8], i.e., the available DoF. In the following, we take planar arrays as an example to derive corresponding DoF.

• *Planar arrays*: Without loss of generality, assuming  $h(x, y, z)$  is observed over a 2D rectangle  $\mathcal{V}_2$  of side lengths  $L_1 > L_2$ , and  $\mathcal{V}_2$  lies in the  $xy$  plane. According to 2D Fourier Plane-Wave Series Expansion,  $h(x, y) = h(x, y, 0)$  is given by

$$h(x, y) \approx \sum_{(l,m) \in \mathcal{E}} c_{l,m} \varphi_{l,m}(x, y) \quad (x, y) \in \mathcal{V}_2 \quad (9)$$

where  $\varphi_{l,m}(x, y) = \varphi_l(x)\varphi_m(y)$  is the 2D Fourier basis, and  $c_{l,m} = \sqrt{L_x L_y} H_{lm}(0)$ . The average number of DoF is limited by the cardinality of  $\{H_{lm}\}$ , which is the number of lattice points falling into the 2D **inner** lattice ellipse shown in Fig. 1, that is its Lebesgue measure of  $\mathcal{E}$ . This yields

$$DoF_{far-field} = \frac{\pi}{\lambda^2} L_x L_y \quad (10)$$

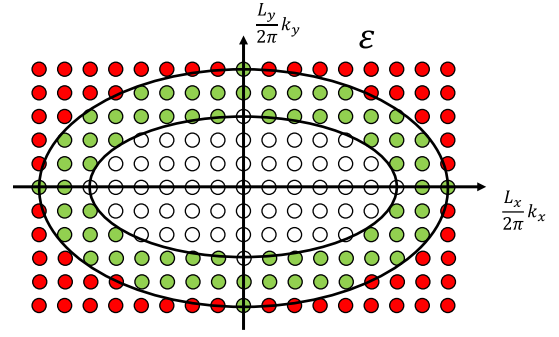


Fig. 1. The 2D lattice ellipse  $\mathcal{E}$  wavenumber spectral support of  $h(x, y, z)$ .

2) *Near-Field Communications*: We now consider evanescent waves for near-field communication and compute the number of DoF over planar aperture spaces.

*Definition 1*: The amplitude of evanescent wave attenuates exponentially with propagation distance and its power can be written as

$$\frac{\mathcal{P}_{receive}}{\mathcal{P}_{send}} = e^{-2k_d d} \quad (11)$$

where  $k_d$  is the modulus of imaginary wavenumber,  $d$  is the propagation distance;  $\mathcal{P}_{receive}$  and  $\mathcal{P}_{send}$  are received power and transmitted electromagnetic power respectively.

*Theorem 1*: The additional DoF can be obtained in the near-field communications is generally given as follow, which vanishes as the distance between the transmitter and receiver planes increases.

$$DoF_{evanescent} = DoF_{far-field} * \frac{1}{(4d\pi)^2} * \lambda^2 * \ln^2 \frac{\mathcal{P}_{send}}{\mathcal{P}_{noise} \cdot 10^{0.1t}} \quad (12)$$

where  $d$  is the propagation distance,  $\lambda$  is wavelength and  $t$  is the received signal-to-noise ratio.

The intuition behind this mathematical equation is that the extra DoF obtained is expected only in the near-field region, whose extension is closely related to the wavelength.

*Proof*: We assume that the impact of evanescent waves is only considered when the received signal-to-noise ratio is larger than  $t$  dB,  $t$  is a parameter depending on the detection ability of the receiver. Noting that this is a general assumption and the main reason for this is to analyze the influence of evanescent waves on DoF and capacity. Without loss of generality, we assume that the transmitting and receiving HMIMO plane are both parallel to  $x - y$  plane. From (11), we can obtain that the largest  $k_z$  satisfies the following equation:

$$10 \cdot \lg \left( \frac{\mathcal{P}_{send} \cdot e^{-2k_z z}}{\mathcal{P}_{noise}} \right) = t$$

then we can calculate  $k_z$  as

$$2k_z z = \ln \left( \frac{\mathcal{P}_{send}}{\mathcal{P}_{noise} \cdot 10^{0.1t}} \right) \\ k_z = \frac{1}{2z} * \ln \left( \frac{\mathcal{P}_{send}}{\mathcal{P}_{noise} \cdot 10^{0.1t}} \right) \quad (13)$$

When the EM wave is evanescent, its wavenumbers on three axes satisfy the following equation:

$$\kappa^2 = k_x^2 + k_y^2 - k_z^2$$

Assuming the outer ellipse in Fig. 1 is defined by

$$t^2 = k_x^2 + k_y^2$$

Then the additional DoF can be calculated by

$$\begin{aligned} DoF_{evanescent} &= DoF_{far-field} * \left( \frac{t^2}{\kappa^2} - 1 \right) \\ &= DoF_{far-field} * \left( \frac{\kappa^2 + k_z^2}{\kappa^2} - 1 \right) \\ &= DoF_{far-field} * \frac{k_z^2}{\kappa^2} \end{aligned} \quad (14)$$

Substituting the corresponding  $k_z$  in (13) into equation (14) with  $\kappa = 2\pi/\lambda$ , (12) can be obtained. ■

### B. Channel Capacity Evaluation

In this section, we analyze channel capacity by considering evanescent waves. Channel capacity in far-field communication scenarios with Fourier series expansion is given by [9]:

$$C = \max_{\mathbf{Q}_a: \text{tr}(\mathbf{Q}_a) \leq 1} \mathbb{E}\{\log_2 \det(\mathbf{I}_{n_r} + \text{snr} \mathbf{H}_a \mathbf{Q}_a \mathbf{H}_a^H)\} \quad (15)$$

where  $\mathbf{Q}_a = \mathbb{E}\{\mathbf{x}_a^H \mathbf{x}_a\}$ , and  $\mathbf{I}_{n_r}$  is an identity matrix of dimension  $n_r$ .  $\mathbf{H}_a \in \mathbb{C}^{n_r \times n_s}$  is the angular response matrix describing the channel coupling between source and receive propagation directions, assuming that there are  $n_s$  and  $n_r$  sampling points on the transmitting and receiving side, respectively. However, Eq. (15) is based on the assumption that  $\tilde{\mathbf{H}}$  is statistically equivalent with  $\mathbf{H}_a$ , which does not hold when considering evanescent waves. Therefore, we will replace  $\mathbf{H}_a$  with  $\tilde{\mathbf{H}}$  to derive the channel capacity in near-field communications. The relation between these two matrixes is in (8).

As shown in Fig. 1, when considering evanescent waves, the angular response matrix can be expanded to include wave-numbers out of 2D lattice ellipse. In other words, sampling points  $n_s$  and  $n_r$  are much more. We assume that channel elements are independent identically distributed (i.i.d), which means the variances of matrix  $\mathbf{H}_a$ 's elements naturally decouple:

$$\sigma^2(l_x, l_y, m_x, m_y) = \sigma_s^2(m_x, m_y) \sigma_r^2(l_x, l_y) \quad (16)$$

where  $\sigma_s^2(m_x, m_y)$  and  $\sigma_r^2(l_x, l_y)$  account for the power transfer at source and receiver, respectively. The corresponding matrix form of variances is:

$$\Sigma = \text{vec}\{\Sigma_r\} \text{vec}\{\Sigma_s\}^H \quad (17)$$

where  $\Sigma_r$  and  $\Sigma_s$  are variance matrices at receiver and source respectively.

To clarify the impact of evanescent waves, we assume  $\Sigma_r = \Sigma_{rin} + \Sigma_{rout}$ , where  $\Sigma_{rin}$  and  $\Sigma_{rout}$  represent variance matrices of sampling points in and out of the traditional support ellipse respectively. As shown in Lemma 1 of work [9], angular random matrix can be obtained by:

$$\mathbf{H}_a = \Sigma \odot \mathbf{W} \quad (18)$$

where  $\mathbf{W}$  is the matrix with i.i.d. circularly-symmetric, complex-Gaussian random entries.

TABLE I  
SIMULATION PARAMETERS

Simulation Parameters	
Antenna linear dimension $D$	Transmission distance
$D = 0.5\text{m}$	$z = 0.5\text{m}^*$
Operation frequency	Power ratio
$f = 3\text{GHz}^*$	$P_{send}/P_{rece} = 125.56\text{dB}^*$

The parameters with\* will be changed in the simulation stage

Thus, the capacity of near-field communications with evanescent waves can be calculated by:

$$C = \max_{\mathbf{Q}_a: \text{tr}(\mathbf{Q}_a) \leq 1} \mathbb{E}\{\log_2 \det(\mathbf{I}_{n_r} + \text{snr} \tilde{\mathbf{H}} \mathbf{Q}_a \tilde{\mathbf{H}}^H)\} \quad (19)$$

where  $\tilde{\mathbf{H}} = \mathbf{e}^{j\Gamma_r} \mathbf{H}_a \mathbf{e}^{-j\Gamma_s}$ .

If the sampling points are in the traditional 2D ellipse region,  $\gamma_r$  and  $\gamma_s$  are real and  $\tilde{\mathbf{H}}$  is statistically equivalent to  $\mathbf{H}_a$ . However, when the sampling points are outside the 2D ellipse region (i.e., evanescent waves are used for transmissions),  $\gamma_r$  and  $\gamma_s$  are imaginary and the signal power decays exponentially with the transmission distance (i.e.,  $\tilde{\mathbf{H}}$  is not statistically equivalent to  $\mathbf{H}_a$ ).

For simplicity, we assume: (a) instantaneous channel state information is only available at the receiver; (b) communications happen only in interior 2D ellipse region or exterior 2D ellipse region (i.e., there is no cross region communications). Under assumption (a), the ergodic capacity in (19) is achieved by an i.i.d input vector  $\mathbf{x}_a$  with  $\mathbf{Q}_a = \frac{1}{n_s} \mathbf{I}_{n_s}$  and channel capacity is given by

$$C = \sum_{i=1}^{\text{rank}(\tilde{\mathbf{H}})} \mathbb{E}\{\log_2(1 + \frac{\text{snr}}{n_s} \lambda_i(\tilde{\mathbf{H}} \tilde{\mathbf{H}}^H))\} \quad (20)$$

where  $\{\lambda_i(\mathbf{A})\}$  are the eigenvalues of an arbitrary  $\mathbf{A}$ . Assuming the transmitting array is on the  $x - y$  plane (i.e.,  $s_z = 0$ ), then (20) can be decomposed into:

$$C = \sum_{i=1}^{\text{rank}(\tilde{\mathbf{H}})} \mathbb{E}\{\log_2[1 + \frac{\text{snr}}{n_s} \lambda_i(e^{j\Gamma_r} \Sigma \odot \mathbf{W} (e^{j\Gamma_r} \Sigma \odot \mathbf{W})^H)]\} \quad (21)$$

Applying (17) and  $\Sigma_r = \Sigma_{rin} + \Sigma_{rout}$ , we can obtain:

$$\Sigma = [\text{vec}(\Sigma_{rin}) + \text{vec}(\Sigma_{rout})][\text{vec}(\Sigma_{sin})^H + \text{vec}(\Sigma_{sout})^H]$$

Under assumption (b), we can simplify the above equation into:

$$\Sigma = \text{vec}(\Sigma_{rin}) \text{vec}(\Sigma_{sin})^H + \text{vec}(\Sigma_{rout}) \text{vec}(\Sigma_{sout})^H \quad (22)$$

The capacity simulation results in Section IV are obtained by plugging (22) into (21).

## IV. SIMULATION RESULTS

Numerical results are performed to validate our theoretical results for rectangular transceiver apertures. Initially, we set simulation parameters as Table I, then the DoF improvement percentage of near-field communications compared to the conventional far-field communication is computed through (12) with one variable varying each time. Note that we assume  $t = 0\text{dB}$  in all the simulations.

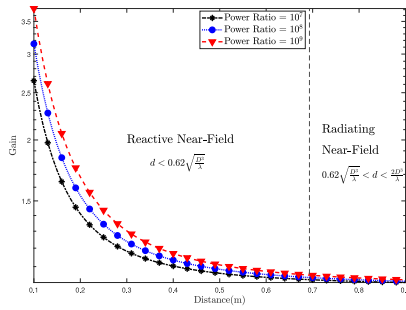


Fig. 2. Improved DoF percentage as a function of transmission distance.

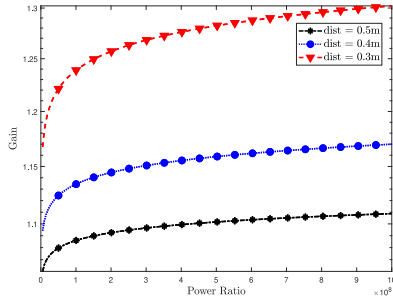


Fig. 3. Improved DoF percentage as a function of the ratio between transmission power and noise power.

TABLE II  
CAPACITY SIMULATION PARAMETERS

Simulation Parameters	
Antenna linear dimension $D$	Operation frequency
$D = 10\lambda$	$f = 300M/900M/3GHz$
Transmission Distance	
$z = 0.01 - 1m^*$	

The parameters with\* will be changed in the simulation stage

In Fig. 2, it is shown that as the transmission distance becomes larger, the additional DoF provided by evanescent waves decreases rapidly. In fact, when the propagation distance exceeds reactive near-field's region, the DoF improvement can be neglected, which validates that the extra DoF gain only be obtained in the reactive near-field region.

In Fig. 3, it is shown that as transmission power increases, extra DoF gain increases rapidly at first but converges to a constant mainly determined by the transmission distance, where the extra DoF gain can achieve more than 30% improvement. This indicates that additional DoF gain is not mainly driven by transmit power consumption, but the EM nature of near-field communication.

Next, we set simulation parameters as Table II, then the channel capacity improvement of near-field communications is computed through (15) and (21).

In Fig. 4, it is shown that as the transmission distance becomes larger, the additional channel capacity provided by evanescent waves decreases rapidly. Moreover, with the increase of the operating frequency, the extra capacity goes down faster. When the receiver goes to the corresponding radiative near-field and farther region, the DoF improvement can be neglected, which further validates that extra DoF benefit can only be obtained in the reactive near-field region.

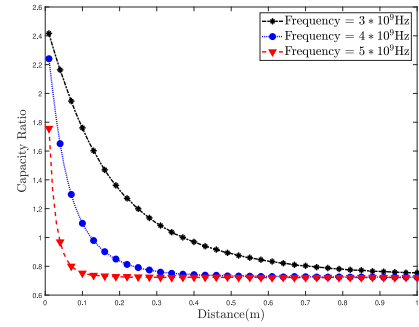


Fig. 4. Improved capacity percentage is a function of transmission distance.

## V. CONCLUSION

Based on the Fourier plane-wave series representation of a spatially-stationary scattering channel, we derived a theoretical DoF and capacity gain in the near-field region by considering evanescent waves. This theoretical result captures the essence of EM propagation and also illuminates the possible benefits brought by evanescent waves. The analysis is limited to an isotropic scattering environment but can be extended to the non-isotropic case through the linear-system theoretic interpretation of plane-wave propagation. Numerical simulations demonstrate the validity of the derivations and its coherence with conventional DoF analysis in the far-field region.

## ACKNOWLEDGMENT

Any opinions, findings and conclusions or recommendations expressed in this material are those of the author(s) and do not reflect the views of the Ministry of Education, Singapore.

## REFERENCES

- [1] C. Huang et al., "Holographic MIMO surfaces for 6G wireless networks: Opportunities, challenges, and trends," *IEEE Wireless Commun.*, vol. 27, no. 5, pp. 118–125, Oct. 2020.
- [2] S. Hu, F. Rusek, and O. Edfors, "Beyond massive MIMO: The potential of data transmission with large intelligent surfaces," *IEEE Trans. Signal Process.*, vol. 66, no. 10, pp. 2746–2758, May 2018.
- [3] A. S. Y. Poon, R. W. Brodersen, and D. N. C. Tse, "Degrees of freedom in multiple-antenna channels: A signal space approach," *IEEE Trans. Inf. Theory*, vol. 51, no. 2, pp. 523–536, Feb. 2005.
- [4] M. Franceschetti, "On Landau's Eigenvalue Theorem and information cut-sets," *IEEE Trans. Inf. Theory*, vol. 61, no. 9, pp. 5042–5051, Sep. 2015, doi: [10.1109/TIT.2015.2456874](https://doi.org/10.1109/TIT.2015.2456874).
- [5] S. S. A. Yuan, Z. He, X. Chen, C. Huang, and W. E. I. Sha, "Electromagnetic effective degree of freedom of a MIMO system in free space," *IEEE Antennas Wireless Propag. Lett.*, vol. 21, no. 3, pp. 446–450, Mar. 2022, doi: [10.1109/LAWP.2021.3135018](https://doi.org/10.1109/LAWP.2021.3135018).
- [6] N. Decarli and D. Dardari, "Communication modes with large intelligent surfaces in the near field," *IEEE Access*, vol. 9, pp. 165648–165666, 2021, doi: [10.1109/ACCESS.2021.3133707](https://doi.org/10.1109/ACCESS.2021.3133707).
- [7] Z. Zhang and L. Dai, "Pattern-division multiplexing for continuous-aperture MIMO," in *Proc. IEEE Int. Conf. Commun.*, 2022, pp. 3287–3292, doi: [10.1109/ICC45855.2022.9839220](https://doi.org/10.1109/ICC45855.2022.9839220).
- [8] A. Pizzo, T. L. Marzetta, and L. Sanguinetti, "Degrees of freedom of holographic MIMO channels," in *Proc. IEEE SPAWC*, 2020, pp. 1–5.
- [9] A. Pizzo, L. Sanguinetti, and T. L. Marzetta, "Fourier plane-wave series expansion for holographic MIMO communications," *IEEE Trans. Wireless Commun.*, vol. 21, no. 9, pp. 6890–6905, Sep. 2022, doi: [10.1109/TWC.2022.3152965](https://doi.org/10.1109/TWC.2022.3152965).
- [10] A. Pizzo, T. L. Marzetta, and L. Sanguinetti, "Spatially-stationary model for holographic MIMO small-scale fading," *IEEE J. Sel. Areas Commun.*, vol. 38, no. 9, pp. 1964–1979, Sep. 2020.
- [11] L. Wei et al., "Multi-user holographic MIMO surfaces: Channel modeling and spectral efficiency analysis," *IEEE J. Sel. Topics Signal Process.*, vol. 16, no. 5, pp. 1112–1124, Aug. 2022, doi: [10.1109/JSTSP.2022.3176140](https://doi.org/10.1109/JSTSP.2022.3176140).